Eur. Phys. J. C 50, 557–571 (2007)
DOI 10.1140/epjc/s10052-007-0215-9

THE EUROPEAN PHYSICAL JOURNAL C

Regular Article – Theoretical Physics

Aspects of radiative K^+_{e3} decays

B. Kubis[1,a], E.H. Müller[1,2], J. Gasser[3], M. Schmid[3]

[1] Helmholtz-Institut für Strahlen- und Kernphysik, Universität Bonn, Nussallee 14–16, 53115 Bonn, Germany
[2] School of Physics, University of Edinburgh, King's Buildings, Mayfield Road, Edinburgh EH9 3JZ, UK
[3] Institut für theoretische Physik, Universität Bern, Sidlerstrasse 5, 3012 Bern, Switzerland

Received: 30 November 2006 /
Published online: 9 February 2007 – © Springer-Verlag / Società Italiana di Fisica 2007

Abstract. We re-investigate the radiative charged kaon decay $K^\pm \to \pi^0 e^\pm \nu_e \gamma$ [$K^\pm_{e3\gamma}$] in chiral perturbation theory, merging the chiral expansion with Low's theorem. We thoroughly analyze the precision of the predicted branching ratio relative to the non-radiative decay channel. Structure dependent terms and their impact on differential decay distributions are investigated in detail, and the possibility to see effects of the chiral anomaly in this decay channel is emphasized.

PACS. 13.20.Eb; 11.30.Rd; 12.39.Fe

1 Introduction

A particularly useful concept for the investigation of radiative processes is the decomposition of the transition amplitudes in an inner bremsstrahlung (IB) and a structure dependent (SD) part. The bremsstrahlung part is non-vanishing (in fact, divergent) in the soft photon limit, and it can be, according to Low's theorem [1], expressed entirely in terms of the corresponding non-radiative amplitude and derivatives thereof; in terms of Feynman diagrams, it corresponds to photon radiation off the external charged particles. Only the structure dependent part contains genuinely new information on the photon coupling to intermediate hadronic states.

Low's theorem was applied to radiative $K_{\ell 3}$ decays in [2, 3]. As is often the case for processes where bremsstrahlung is not forbidden by some mechanism, the IB part of the amplitude was found to be largely dominant in the partial decay widths, and so several of the earlier studies (see e.g. [4]) rather concentrated on precision tests of soft photon theorems. Only with the advent of modern high-statistics kaon decay experiments has it become feasible to measure a relatively rare decay channel to the required precision such as to even find effects of structure dependent contributions.

Experiments typically concern the branching ratio relative to the corresponding non-radiative process $K^\pm \to \pi^0 e^\pm \nu_e$ [$K^\pm_{e3}$],

$$R\left(E_\gamma^{\rm cut},\, \theta_{e\gamma}^{\rm cut}\right) = \frac{\Gamma\left(K^\pm_{e3\gamma},\, E^*_\gamma > E_\gamma^{\rm cut},\, \theta^*_{e\gamma} > \theta_{e\gamma}^{\rm cut}\right)}{\Gamma\left(K^\pm_{e3}\right)}\,, \quad (1)$$

where a minimal photon energy $E_\gamma^{\rm cut}$ as well as a minimal photon–positron opening angle $\theta_{e\gamma}^{\rm cut}$ (both in the kaon rest frame) are specified.

Experimental results for the relative branching ratios R for $K^\pm_{e3\gamma}$ are shown in Table 1, where we display the dependence on the angular cut in degrees, although in some of the original publications only the cosine is mentioned. Reference [5] also includes values for R with different photon energy cuts (but always for the same angular interval). One should note that the results of the analysis in [6] explicitly refer to the decay probability of an inner bremsstrahlung radiative process. We have omitted earlier experimental data in Table 1, with statistics determined by less than 20 candidate events [9, 10].

New experimental efforts that ought to supersede most of the previous results are under way at NA48/2 [11] and KEK-E470 [12], and ought to record more detailed information than just the partial widths, in particular precise photon energy distributions in order to extract information on structure dependent terms. They are likely to signifi-

Table 1. Experimental values of R for the decay $K^\pm_{e3\gamma}$. A single value for the angle cut $\theta_{e\gamma}^{\rm cut}$ denotes a minimal photon–lepton angle, while ranges refer to minimal and maximal values

Ref.	$E_\gamma^{\rm cut}$	$\theta_{e\gamma}^{\rm cut}$	events	$R \times 10^2$
[5]	10 MeV	26–53°	192	0.56 ± 0.04
[6, 7]	10 MeV	26–53°	82	0.46 ± 0.08
[6, 7]	10 MeV	10°	82	1.51 ± 0.25
[8]	10 MeV	[none]	3852	$1.69 \pm 0.03 \pm 0.07$
[8]	10 MeV	26–53°	1423	$0.48 \pm 0.02 \pm 0.03$
[8]	30 MeV	20°		$0.63 \pm 0.02 \pm 0.03$

[a] e-mail: kubis@itkp.uni-bonn.de

cantly surpass the statistics obtained in the most recent measurements of the corresponding neutral kaon decay mode $K_{\rm L}\to\pi^\mp e^\pm\nu_e\gamma$ [$K^0_{e3\gamma}$] [13–15], therefore more precise results on structure dependent terms in $K^+_{e3\gamma}$ ought to be feasible than obtained for those in $K^0_{e3\gamma}$ in the pioneering investigation of [13].

The appropriate theoretical tool to match such experimental refinements is chiral perturbation theory (ChPT) [16, 17], the effective field theory of the standard model at low energies. Radiative $K_{\ell3}$ decays were calculated up to order p^4 in the chiral expansion in [18] (see also [19] for an earlier tree-level calculation), and in [20] this work was extended and combined with the useful aspects of the Low expansion for $K^0_{e3\gamma}$. It is the aim of the present article to apply the ideas and methods developed in [20] to $K^+_{e3\gamma}$ decays. In Sect. 2, we present the necessary formalism on the $K^+_{e3\gamma}$ decay amplitudes, in particular the IB–SD separation. ChPT results on structure dependent terms are discussed analytically and numerically in Sect. 3, where in particular we present the complete $\mathcal{O}(p^6)$ results for the axial amplitudes. In Sect. 4, we derive our prediction for the ratio of branching ratios R and give a detailed account of the uncertainties in such a prediction. Section 5 discusses the possibility to extract information on structure dependent terms from differential decay distributions, and in particular on the axial anomaly in this decay. Finally, we summarize our findings in Sect. 6.

In this work, we disregard the interesting topic of T-odd correlations in $K^+_{e3\gamma}$ decays, which was discussed in detail in [21–23].

2 Formalism

In the following, we consider the decay channel

$$K^+(p)\to\pi^0(p')\,e^+(p_e)\,\nu_e(p_\nu)\,\gamma(q)\qquad[K^+_{e3\gamma}]\qquad(2)$$

and its charge conjugate mode. We only study the emission of a real photon; that is, $q^2=0$.

2.1 The decay amplitude

The transition matrix element for $K^+_{e3\gamma}$ has the form

$$\begin{aligned}T\left(K^+_{e3\gamma}\right)&=\frac{G_{\rm F}}{\sqrt{2}}\,e\,V^*_{us}\,\epsilon^\mu(q)^*\\&\quad\times\Big[\left(V_{\mu\nu}-A_{\mu\nu}\right)\bar u(p_\nu)\,\gamma^\nu\,(1-\gamma_5)\,v(p_e)\\&\quad+\frac{F_\nu}{2p_eq}\,\bar u(p_\nu)\,\gamma^\nu\,(1-\gamma_5)\left(m_e-\not{p}_e-\not{q}\right)\gamma_\mu\,v(p_e)\Big]\\&\doteq\epsilon^\mu(q)^*\,M_\mu\,.\end{aligned}\qquad(3)$$

The relevant diagrams are displayed in Fig. 1.

The first term of (3) corresponds to diagram a), which includes bremsstrahlung off the charged kaon, while the second one corresponds to the radiation off the positron, represented by diagram b). We have introduced the hadronic tensors $V_{\mu\nu}$ and $A_{\mu\nu}$,

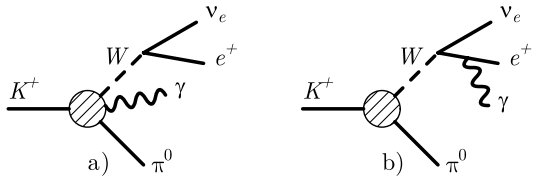

Fig. 1. Diagrams describing $K^+_{e3\gamma}$ decay

$$\begin{aligned}I_{\mu\nu}&=\mathrm{i}\int\mathrm{d}^4x\,\mathrm{e}^{\mathrm{i}qx}\,\left\langle\pi^0\left(p'\right)|T\,V^{\rm em}_\mu(x)\,I^{\rm had}_\nu(0)|K^+(p)\right\rangle\,,\\I&=V,A\,,\end{aligned}\qquad(4)$$

with

$$\begin{aligned}V^{\rm had}_\nu&=\overline{s}\gamma_\nu u\,,\quad A^{\rm had}_\nu=\overline{s}\gamma_\nu\gamma_5 u\,,\\V^{\rm em}_\mu&=(2\overline{u}\gamma_\mu u-\overline{d}\gamma_\mu d-\overline{s}\gamma_\mu s)/3\,,\end{aligned}\qquad(5)$$

whereas F_ν is the K^+_{e3} matrix element

$$F_\nu=\langle\pi^0(p')|V^{\rm had}_\nu(0)|K^+(p)\rangle\,.\qquad(6)$$

The tensors $V_{\mu\nu}$ and $A_{\mu\nu}$ satisfy the Ward identities

$$q^\mu V_{\mu\nu}=F_\nu\,,\qquad q^\mu A_{\mu\nu}=0\,,\qquad(7)$$

which imply gauge invariance of the total amplitude (3),

$$q^\mu M_\mu=0\,.\qquad(8)$$

The $K^+_{e3\gamma}$ amplitude can be decomposed into inner bremsstrahlung and structure dependent parts. We require these two amplitudes to be separately gauge invariant and the SD part to be of order q and higher in an expansion in powers of the photon momenta. According to Low's theorem [1], the IB terms, which comprise the part of the amplitude non-vanishing for small photon momenta (and in particular the infrared divergent pieces), are given entirely in terms of the K^+_{e3} form factors f_+, f_1 defined by

$$F_\nu(t)=\frac{1}{\sqrt{2}}\Big(2p'_\nu f_+(t)+(p-p')_\nu f_1(t)\Big)\,,\qquad(9)$$

with $t=(p-p')^2$. [We use the form factors f_+, f_1 instead of the more conventional f_+, $f_-=f_1-f_+$ in order to be able to write the IB amplitude in a slightly more compact form below.] This splitting of the matrix element implies a corresponding splitting of the hadronic tensors $V_{\mu\nu}$ and $A_{\mu\nu}$. The axial correlator $A_{\mu\nu}$ consists of structure dependent parts only, and can be expressed in terms of four scalar functions A_i, $i=1\ldots4$,

$$\begin{aligned}A_{\mu\nu}=\frac{\mathrm{i}}{\sqrt{2}}\Big[&\epsilon_{\mu\nu\rho\sigma}\left(A_1\,p'^\rho q^\sigma+A_2\,q^\rho W^\sigma\right)\\&+\epsilon_{\mu\lambda\rho\sigma}\,p'^\lambda q^\rho W^\sigma\left(\frac{A_3}{M_K^2-W^2}\,W_\nu+A_4\,p'_\nu\right)\Big]\,,\end{aligned}\qquad(10)$$

where $W = p - p' - q$. (We use the convention $\epsilon_{0123} = +1$.) Note that in comparison to [18,20], we have factored out the kaon pole explicitly in the definition of the structure function A_3.

The decomposition of the vector correlator reads

$$V_{\mu\nu} = V^{\rm IB}_{\mu\nu} + V^{\rm SD}_{\mu\nu} \,, \tag{11}$$

where the SD piece is chosen such that

$$q^\mu V^{\rm IB}_{\mu\nu} = F_\nu(t) \,, \quad q^\mu V^{\rm SD}_{\mu\nu} = 0 \,. \tag{12}$$

For a given choice of $V^{\rm SD}_{\mu\nu}$, the structure dependent part of the decay amplitude T in (3) is defined to be

$$\begin{aligned} T^{\rm SD} = {} & \frac{G_{\rm F}}{\sqrt{2}}\, e\, V_{us}^*\, \epsilon^\mu(q)^* \left(V^{\rm SD}_{\mu\nu} - A_{\mu\nu}\right) \\ & \times \bar u(p_\nu)\, \gamma^\nu\, (1-\gamma_5)\, v(p_e) \,, \end{aligned} \tag{13}$$

whereas the bremsstrahlung part is $T^{\rm IB} = T - T^{\rm SD}$.

It remains to explicitly construct the decomposition (11). This is done explicitly in Appendix A, where we derive the form of $V^{\rm IB}_{\mu\nu}$ in terms of f_+ and f_1 as

$$\begin{aligned} V^{\rm IB}_{\mu\nu} = {} & \frac{1}{\sqrt{2}} \Bigg[\frac{p_\mu}{pq} \left(2p'_\nu f_+\left(W^2\right) + W_\nu f_1\left(W^2\right)\right) \\ & + \frac{W_\mu}{qW} \left(2p'_\nu \Delta f_+ + W_\nu \Delta f_1\right) + g_{\mu\nu} f_1(t) \Bigg] \,, \\ \Delta f_i = {} & f_i(t) - f_i\left(W^2\right) \,, \quad i = +, 1 \,. \end{aligned} \tag{14}$$

A slightly different representation for the IB amplitude was already derived in [2,3]. It differs from the one given above by terms of order q. An important feature of the form (14) is the fact that it contains all singularities at $pq = 0$ in the sense that the complete residue at $pq = 0$, which is a non-trivial function of the momenta p, p', and q, is contained in it, and no terms like $(qW)^2/pq$ (which is formally of order q) are shifted to the structure dependent tensor.

The structure dependent part of the vector correlator can also be expressed in terms of four scalar functions V_i, $i = 1 \ldots 4$, in a basis of gauge invariant tensors according to [24]

$$\begin{aligned} V^{\rm SD}_{\mu\nu} = {} & \frac{1}{\sqrt{2}} \Big[V_1 \left(p'_\mu q_\nu - p'q\, g_{\mu\nu}\right) + V_2 \left(W_\mu q_\nu - qW\, g_{\mu\nu}\right) \\ & + V_3 \left(qW\, p'_\mu W_\nu - p'q\, W_\mu W_\nu\right) \\ & + V_4 \left(qW\, p'_\mu p'_\nu - p'q\, W_\mu p'_\nu\right) \Big] \,. \end{aligned} \tag{15}$$

2.2 Kinematics

We briefly collect the essential information on the kinematics of this decay. The Lorentz invariant amplitudes A_i, V_i are functions of three scalar variables, which we often take to be

$$s = (p'+q)^2 \,, \quad t = (p-p')^2 \,, \quad u = (p-q)^2 \,. \tag{16}$$

These variables are particularly useful in the discussion of the analytic properties of V_i, A_i. The physical region in $K_{e3\gamma}$ decays can be represented as follows: for fixed W^2, the variables s, t, and u vary in the range

$$\begin{aligned} & W^2 \le t \le (M_K - M_\pi)^2 \,, \\ & s_- \le s \le s_+ \,, \\ & s_\pm = M_\pi^2 - \frac{1}{2t}\left(t + M_\pi^2 - M_K^2\right)\left(t - W^2\right) \\ & \qquad \pm \frac{1}{2t} \lambda^{1/2}\left(t, M_K^2, M_\pi^2\right) \lambda^{1/2}\left(t, 0, W^2\right) \,, \\ & s + t + u = M_K^2 + M_\pi^2 + W^2 \,, \end{aligned} \tag{17}$$

where λ is the usual Källén function,

$$\lambda(x,y,z) = x^2 + y^2 + z^2 - 2(xy + xz + yz) \,. \tag{18}$$

Note that $M_\pi^2 = M_{\pi^0}^2$ denotes the neutral pion mass in this work. Varying the invariant mass squared W^2 of the lepton pair in the interval

$$m_e^2 \le W^2 \le (M_K - M_\pi)^2 \tag{19}$$

generates the region covered by s, t, u in $K_{e3\gamma}$ decays. Instead of s, t, u, we also use

$$pq/M_K = E_\gamma^* \,, \quad pp'/M_K = E_\pi^* \,, \quad W^2 = (p_e + p_\nu)^2 \,, \tag{20}$$

where E_γ^*, E_π^* are the photon and the pion energy in the kaon rest frame. These variables are often useful when discussing partial decay widths.

For the four-body decay $K^+_{e3\gamma}$, one needs five independent variables to describe the kinematics of the decay completely. We choose the two additional scalar products

$$pp_e/M_K = E_e^* \,, \quad x = p_e q/M_K^2 \,, \tag{21}$$

where E_e^* is the positron energy in the kaon rest frame. The dimensionless variable x is related to the angle $\theta^*_{e\gamma}$ between the photon and the positron:

$$xM_K^2 = E_\gamma^* \left(E_e^* - \sqrt{E_e^{*2} - m_e^2}\, \cos\theta^*_{e\gamma}\right) . \tag{22}$$

The smallness of the electron mass leads to a near-vanishing of x for collinear electron and photon momenta, and hence to a near-singularity, which is avoided by cutting on the angle $\theta^*_{e\gamma}$.

The total decay rate is given by

$$\begin{aligned} & \Gamma(K^+ \to \pi^0 e^+ \nu\gamma) \\ & \quad = \frac{1}{2M_K (2\pi)^8} \int {\rm d}_{\rm LIPS}(p;\, p', p_e, p_\nu, q) \sum_{\rm spins} |T|^2 \,, \end{aligned} \tag{23}$$

where ${\rm d}_{\rm LIPS}(p; p', p_e, p_\nu, q)$ is the Lorentz invariant phase space element for the $K^+_{e3\gamma}$ process.[1] When performing

[1] For the decay of a particle of momentum p into n particles of momenta $p_1, \ldots, p_n$, one has

$${\rm d}_{\rm LIPS}(p; p_1, \ldots, p_n) = \delta^4\left(p - \sum_{i=1}^n p_i\right) \prod_{k=1}^n \frac{{\rm d}^3 p_k}{2p_k^0} \,.$$

the traces over the spins, we work with massless spinors, such that the form factors A_3, V_3, and f_1 drop out, and $\sum_{\text{spins}} |T|^2$ is a bilinear form of the invariant amplitudes V_i, A_i, $i = 1, 2, 4$, and f_+. The explicit result is displayed in Appendix B.

3 Structure dependent terms in ChPT

3.1 Analytical results at order p^4

In [18], the chiral expansion was carried out to order p^4 for both the neutral and the charged decay modes (one-loop order). We do not describe that calculation in any detail and only quote the result, adjusted to the separation between bremsstrahlung and structure dependent terms. The axial amplitudes are given in terms of the Wess–Zumino–Witten anomaly term [25, 26], the result is

$$A_1 = -4A_2 = A_3 = -\frac{1}{2\pi^2 F^2}\,, \quad A_4 = 0 \quad \left[\mathcal{O}\left(p^4\right)\right]. \quad (24)$$

The vector structure functions V_i were shown to be given as

$$V_1 = \sqrt{2} I_2\,, \quad V_2 = -\frac{\sqrt{2}}{qW}\left(I_1 + p'q\, I_2\right),$$
$$V_3 = \frac{\sqrt{2}}{qW}\left(I_3 - f_2^+\left(W^2\right)\right), \quad V_4 = 0 \qquad \left[\mathcal{O}\left(p^4\right)\right], \quad (25)$$

where the functions I_i, $f_2^+(W^2)$ are defined in [18].

It was pointed out in [18] that these functions are real throughout the physical region. In fact, cuts only start at $t = (M_K + M_\pi)^2$, $W^2 = (M_K + M_\pi)^2$, therefore far from the phase space boundaries, which is why the V_i at this order are smooth and well-behaved, and even constant to a high degree of accuracy. They can therefore be approximated by a seemingly drastic simplification, namely by their values at the special kinematical point $s = M_\pi^2$, $u = M_K^2$, $t = W^2 = 0$. This corresponds to an expansion to leading order in the photon momentum q, plus setting $t = 0$. The rather compact and simple result reads

$$\begin{aligned}
V_1 = &-\frac{8}{F^2}\bar{L}_9 - \frac{(1-x)^{-2}}{32\pi^2 F^2}\left\{\frac{1}{3}\left(53 - 25x + 2x^2\right)\right.\\
&+\left(1 + x - x^2 + x^3\right)\frac{\log x}{2(1-x)}\\
&\left.-\left(127 - 93x + 21x^2 - x^3\right)\frac{\log y}{2(1-x)}\right\}\\
&+\mathcal{O}(q,t)\,,\\
V_2 = &-\frac{4}{F^2}\left(\bar{L}_9 + \bar{L}_{10}\right)\\
&-\frac{(1+x)(1-x)^{-2}}{64\pi^2 F^2}\left\{1 + x + \frac{2x\log x}{1-x}\right\}\\
&-\frac{(1-x)^{-3}}{32\pi^2 F^2}\left\{\frac{166}{3}(9-4x) + (77-x)\frac{x^2}{3}\right.\\
&\left.+x(3+2x)\frac{\log x}{1-x} - 9(12-x)(4-x)^2\frac{\log y}{1-x}\right\}\\
&+\mathcal{O}(q,t)\,,
\end{aligned}$$

$$\begin{aligned}
V_3 = &-\frac{(1-x)^{-4}}{32\pi^2 F^2 M_K^2}\left\{\frac{2611}{3} - 13x(34-5x) - \frac{4}{3}x^3\right.\\
&\left.+x(2+3x+x^2)\frac{\log x}{1-x} - 27(7-x)(4-x)^2\frac{\log y}{1-x}\right\}\\
&+\mathcal{O}(q,t)\,, \qquad (26)
\end{aligned}$$

where $x = M_\pi^2/M_K^2$, $y = M_\eta^2/M_K^2$, and we have made frequent use of the Gell-Mann–Okubo relation. See (D.6) for a definition of the scale independent low-energy constants $\bar{L}_9$, $\bar{L}_{10}$. We remark that the expressions for V_1 and V_3 in (26) are identical to the equivalent approximations in the neutral kaon decay mode quoted in [20].

3.2 Analytical results at order p^6

As the above-described results for the structure functions V_i, A_i at $\mathcal{O}(p^4)$ are the leading contributions in the chiral expansion, and as the chiral expansion involving strangeness does not necessarily converge very fast, it is mandatory to understand the structure of higher-order corrections in order to give realistic estimates of the structure dependent terms.

The analytic structure of the tensors $V_{\mu\nu}$, $A_{\mu\nu}$ was investigated in detail in [20, 23]. The main results of those investigations are as follows.

1. Due to strangeness conservation, cuts in the variables t, u, W^2 can all start only at $(M_K + M_\pi)^2$, which is far outside the physical region. As in the case of the vector structure functions at $\mathcal{O}(p^4)$, these cuts are expected to hardly affect the momentum dependence of the V_i, A_i inside the decay region, where they can therefore be approximated by polynomials.
2. At higher order in the chiral expansion, there are two- and three-pion cuts in the s-channel that make the structure functions complex. These cuts were discussed in great detail in [23]. Due to the photon in the final state, all the diagrams developing imaginary parts have a P-wave characteristic, i.e. the imaginary parts rise only slowly above threshold, and a cusp-like structure in the real parts is smoothed out ($\propto (s - 4M_\pi^2)^{3/2}$ in the case of the two-pion cuts). For our purposes, the real parts of the structure functions can therefore still be regarded as "smooth".

The main purpose of the analysis of higher-order corrections is therefore to see how large the corrections to the averaged (constant) structure functions might be.

3.2.1 Complete order p^6 corrections to the axial amplitudes

We have calculated the complete $\mathcal{O}(p^6)$ corrections to the axial structure functions A_1, A_2, and A_4. The contribution of A_3 to the squared matrix element is always suppressed by a factor of $m_e^2/M_K^2 \approx 10^{-6}$ and is therefore neglected. The generic structure is as follows:

$$A_1 = -\frac{1}{2\pi^2 F_\pi F_K}\left\{1 + S_1(s) + T_1(t) + U_1(u) + X_1\right\},$$
$$A_2 = \frac{1}{8\pi^2 F_\pi F_K}\left\{1 + S_2(s) + T_2(t) + U_2(u) + X_2\right\},$$

$$A_4 = -\frac{C_{4A}}{F_\pi F_K}\,. \tag{27}$$

The explicit forms for the various loop functions as well as the combinations of low-energy constants entering the expressions (27) can be found in Appendix C. In particular, the constant terms $X_{1,2}$ in (27) contain terms proportional to the strange quark mass, and are therefore potentially big. We remark that by renormalizing the order p^4 amplitudes according to $F^2 \to F_\pi F_K$, all dependence on the low-energy constants L_4 and L_5 is absorbed in the physical meson decay constants.

3.2.2 Polynomial corrections to the vector amplitudes

A complete evaluation of the vector structure functions at order p^6 requires a full two-loop calculation and is beyond the scope of this article. In order to gain a basic idea about potential higher-order corrections, we content ourselves with an investigation of just polynomial contributions. Note that the loop contributions with cuts in the physical region are known to be tiny at this order [23].

The polynomial part for the V_i can be calculated from the Lagrangian $\mathcal{L}_6$ [27,28]. For the form factors V_1, V_2, it contains all possible terms linear in s, t, u, W^2, M_K^2, M_π^2. The numerically potentially largest corrections for V_1, V_2 turn out to be the terms suppressed by a factor $M_K^2/(4\pi F)^2$ with respect to the leading $\bar{L}_9$, $\bar{L}_{10}$ contributions. The (leading) polynomial contributions for V_3, V_4, which only appear at $\mathcal{O}(p^6)$, are constant.

We have furthermore calculated the contributions of the form $L_i \times L_j$ at order p^6. In analogy to what was done above for the axial structure functions, we find that a renormalization of the order p^4 couplings according to $F^2 \to F_\pi F_K$ takes care of all such terms. This information is used for the numerical evaluation of the structure functions below, where such a normalization is chosen in order to minimize higher-order corrections.

3.3 Numerical evaluation of structure dependent terms

In Table 2, we summarize the numerical evaluation of the various structure dependent terms. We use the parameters and numerical values specified in Appendix D. In particular, we neglect any variation in the order p^4 low-energy constants L_9, L_{10}, the effect of which should be generously covered by the uncertainty in the order p^6 contributions estimated below.

The averages $\langle V_i\rangle$, $\langle A_i\rangle$ in the first column of Table 2, referring to the values of the structure dependent terms at order p^4, are obtained by integrating the structure functions over phase space and dividing by the phase space volume; the quoted uncertainties are the 1σ errors of this averaging procedure. These are therefore no realistic estimates of the uncertainties of the mean values, but they only serve as an illustration of to what extent the approximation of the V_i being constant at this order is justified. It is seen that the variation within physical phase space is absolutely negligible. This is, on the one hand, due to the absence of cuts, but also to the fact that V_1 and V_2 are (at the scale of the ρ mass) numerically dominated by counterterm contributions, which are in turn necessarily constant at this order. For comparison, we also show the values of the V_i at the special kinematical point $s = M_\pi^2$, $u = M_K^2$, $t = W^2 = 0$ as given in (26), which are consistent with this picture.

Table 2. Values for the structure dependent terms as given by $\mathcal{O}(p^4)$ and estimated from $\mathcal{O}(p^6)$ ChPT. The symbols $\langle V_i\rangle$, $\langle A_i\rangle$ denote the averages of the real parts of the V_i, A_i over phase space, in units of M_K. For the V_i, we also show the approximation given in (26). For the error bands, see discussion in main text

	$\mathcal{O}(p^4)$	(26)	$\mathcal{O}(p^6)$
$\langle V_1\rangle$	-1.24 ± 0.004	-1.23	-1.24 ± 0.4
$\langle V_2\rangle$	-0.19 ± 0.007	-0.21	-0.19 ± 0.2
$\langle V_3\rangle$	-0.02 ± 0.001	-0.02	± 0.1
$\langle V_4\rangle$	0	0	± 0.1
$\langle A_1\rangle$	-1.19		-1.29 ± 0.4
$\langle A_2\rangle$	0.30		0.33 ± 0.1
$\langle A_3\rangle$	-1.19		
$\langle A_4\rangle$	0		± 0.3

A numerical assessment of the corrections at next-to-leading order (p^6) is much more difficult, essentially due to the large number of unknown low-energy constants. For the axial structure functions that we have calculated completely, we proceed as follows: by averaging the (real parts of) the loop contributions at a scale $\mu = M_\rho$ over phase space, we calculate the shifted mean values $\langle A_i\rangle$; the counterterm contributions are added as the essential uncertainty. This uncertainty is determined by examining the scale dependence of the combined counterterm contributions. If the scale is varied such that the corresponding logarithms change by one, we find for the counterterm parts of $A_{1,2}$

$$\begin{aligned} A_{1,\mathrm{ct}} &= \mp\frac{1}{192\pi^4 F_\pi^2 F_K^2}\Big\{14\big(M_K^2 - M_\pi^2\big) + 4s + t + u\Big\}\,,\\ A_{2,\mathrm{ct}} &= \pm\frac{1}{768\pi^4 F_\pi^2 F_K^2}\Big\{17M_K^2 - 9M_\pi^2 - 7t + 4u\Big\}\,. \end{aligned} \tag{28}$$

As there are no loop contributions to A_4, the corresponding counterterm combination is separately scale independent, and we have to utilize an even simpler order-of-magnitude estimate with the result

$$A_{4,\mathrm{ct}} = \pm\frac{16}{(4\pi)^4 F_\pi^2 F_K^2}\,. \tag{29}$$

In order to obtain simple error ranges for $\langle A_{1,2}\rangle$, we again average the momentum dependent terms over phase space. It is seen that the largest contributions to the uncertainty stem from constant terms $\propto M_K^2$. In this sense, within the accuracy at which these structure functions can presently be predicted, we can even neglect the momentum dependence and approximate the structure functions by constants.

The results thus obtained for the A_i are displayed in the third column of Table 2. We note that the uncertainties for $A_{1,2}$ are of the size of typical chiral $SU(3)$ corrections of about 30%.

For the V_i, we use the same order-of-magnitude arguments concerning higher-order contributions as in [20]. The uncertainty for the dominant structure function V_1 is estimated to be of the order of 30%; as V_2 is suppressed at leading order, we scale its uncertainty by a factor of 2. The (constant) counterterm contributions to $V_{3,4}$ are estimated by dimensional arguments similar to that for A_4 discussed above. All the numbers are collected in the third column of Table 2.

4 The ratio R

The ratio R defined in (1) is a particular useful quantity to consider in $K_{e3\gamma}$ decays, as it is both the quantity that is naturally measured in experiment (as opposed to the branching ratio $\Gamma(K_{e3\gamma})/\Gamma_{\mathrm{all}}$), and it can be predicted in a clean way theoretically.

We repeat here the corresponding discussion of R for the neutral kaon decay in [20] for the decay channel $K^+_{e3\gamma}$. As the layout of the formalism is analogous to the neutral channel, we shall be rather brief and only comment in more detail on the numerical results.

For the moment, we neglect radiative corrections and isospin breaking and denote R in the absence of virtual and real photon corrections by $\mathcal{R}$,

$$\alpha^{-1}\mathcal{R} = \left[\alpha^{-1}R\right]_{\alpha=0} . \tag{30}$$

We will comment on radiative corrections in Sect. 4.4.

We define the quantity $\overline{\mathrm{SM}}$ by

$$\Gamma(K^+_{e3\gamma}) \doteq \frac{4\alpha M_K^5 G_{\mathrm{F}}^2 |V_{us}|^2}{(2\pi)^7} f_+(0)^2 \int \mathrm{d}_{\mathrm{LIPS}}\, \overline{\mathrm{SM}} , \tag{31}$$

such that $\int \mathrm{d}_{\mathrm{LIPS}}\, \overline{\mathrm{SM}}$ is dimensionless and contains no further (electroweak) coupling constants. By factoring out $f_+(0)^2$, $\overline{\mathrm{SM}}$ only contains the normalized form factor $\bar{f}_+(t) = f_+(t)/f_+(0)$. The non-radiative width $\Gamma(K^+_{e3})$ is conventionally written as

$$\begin{aligned}\Gamma(K^+_{e3}) &= \int \mathrm{d}y\, \mathrm{d}z\, \rho(y,z) ,\\ \rho(y,z) &= \frac{M_K^5 G_{\mathrm{F}}^2 |V_{us}|^2}{256\pi^3} f_+(0)^2 A(y,z) \bar{f}_+(t)^2 ,\end{aligned} \tag{32}$$

where $y = 2pp_e/M_K^2$, $z = 2pp'/M_K^2$, and

$$\begin{aligned}A(y,z) = {}& 4(z+y-1)(1-y) + r_e(4y+3z-3)\\ & - 4r_\pi + r_e(r_\pi - r_e) ,\end{aligned} \tag{33}$$

with $r_e = m_e^2/M_K^2$, $r_\pi = M_\pi^2/M_K^2$. The expression for $\mathcal{R}$ in terms of these reduced phase space integrals is then of the same form as for the neutral decay mode [20],

$$\mathcal{R} = \frac{8\alpha}{\pi^4} \frac{\int \mathrm{d}_{\mathrm{LIPS}}\, \overline{\mathrm{SM}}}{\int \mathrm{d}y\, \mathrm{d}z\, A(y,z) \bar{f}_+(t)^2} . \tag{34}$$

Table 3. Coefficients for the K^+_{e3} phase space integral

a_0	a_1	a_2	a_3	a_4
0.09653	0.3337	0.4618	3.189	6.278

Table 4. Coefficients for the $K^+_{e3\gamma}$ phase space integral

b_0^{IB}	b_1^{IB}	b_2	b_3^{IB}	b_4	b_5
1.019	3.98	5.81	11.83	41.9	84.8
b_0^{SD}		b_1^{SD}		b_3^{SD}	
-0.012 ± 0.004		-0.03 ± 0.01		-0.10 ± 0.03	

We will occasionally also refer to a ratio $\mathcal{R}^{\mathrm{IB}}$, which is understood to be calculated according to (34), with all structure dependent contributions in $\overline{\mathrm{SM}}$ omitted.

4.1 Phase space integrals

Assuming[2]

$$\bar{f}_+(t) = 1 + \lambda_+ \frac{t}{M_{\pi^\pm}^2} + \lambda_+'' \frac{t^2}{M_{\pi^\pm}^4} , \tag{35}$$

one may expand the integral in the denominator according to

$$\begin{aligned}I &= \int \mathrm{d}y\, \mathrm{d}z\, A(y,z) \bar{f}_+(t)^2\\ &= a_0 + a_1\lambda_+ + a_2\left(\lambda_+^2 + 2\lambda_+''\right) + a_3\lambda_+\lambda_+'' + a_4 {\lambda_+''}^2 ,\end{aligned} \tag{36}$$

where the numerical values for the a_i are collected in Table 3. We point out that we have used the physical (charged) kaon and (neutral) pion masses everywhere, such that the kinematics in the phase space integral correspond to the physical situation.

Similarly we can expand the phase space integral for the radiative decay in terms of K_{e3} form factor parameters according to

$$\begin{aligned}I^\gamma &= \int \mathrm{d}_{\mathrm{LIPS}}\, \overline{\mathrm{SM}}\\ &= b_0 + b_1\lambda_+ + b_2\lambda_+^2 + b_3\lambda_+'' + b_4\lambda_+\lambda_+'' + b_5 {\lambda_+''}^2 .\end{aligned} \tag{37}$$

The integral I^γ and the coefficients b_i depend on the experimental cuts E_γ^{cut}, $\theta_{e\gamma}^{\mathrm{cut}}$. The numerical results for the standard cuts $E_\gamma^{\mathrm{cut}} = 30\,\mathrm{MeV}$, $\theta_{e\gamma}^{\mathrm{cut}} = 20^\circ$ are displayed in Table 4. Where applicable, the coefficients have been decomposed into their bremsstrahlung and their structure

[2] Note that, while we use $M_\pi = M_{\pi^0}$ elsewhere in this text, the expansion of the form factor f_+ is conventionally normalized to the charged pion mass $M_{\pi^\pm}$.

dependent parts. The relative size of the structure dependent contributions as predicted by ChPT is very similar to the neutral kaon decay channel, they reduce the width by about 1%. The uncertainties quoted in Table 4 refer to the estimated higher-order contributions in the structure dependent terms as discussed in Sect. 3.3.

4.2 Form factor dependence of $\mathcal{R}$

We can now study the dependence of $\mathcal{R}$ ($\mathcal{R}^{\rm IB}$) on the form factor parameters $\bar\lambda_+ = \lambda_+/\lambda_+^{\rm c}$, $\bar\lambda''_+ = \lambda''_+/(\lambda_+^{\rm c})^2$, where we choose $\lambda_+^{\rm c} = 0.0294$ as a central value for the slope parameter λ_+. We expand $\mathcal{R}$ according to

$$\mathcal{R}\left(\bar\lambda_+, \bar\lambda''_+\right) = \mathcal{R}(1,0)\Big\{1 + c_1\,\left(\bar\lambda_+ - 1\right) + c_2\,\left(\bar\lambda_+ - 1\right)^2 + c_3\,\bar\lambda''_+ + \ldots\Big\}\,, \tag{38}$$

and $\mathcal{R}^{\rm IB}$ accordingly (with expansion coefficients $c_i^{\rm IB}$). We show the numbers for the coefficients c_i, $c_i^{\rm IB}$ in Table 5. We find that although there is a significant cancellation between the λ_+, λ''_+ dependence of numerator and denominator, the cancellation is not quite as complete as for the $K^0_{e3(\gamma)}$ channel [20]. Going from a point-like form factor ($\lambda_+ = 0$) to the physical one $\lambda_+ = \lambda_+^{\rm c}$ induces a change of about 1.3% in $\mathcal{R}$ or $\mathcal{R}^{\rm IB}$.

On the other hand, $\mathcal{R}$ and $\mathcal{R}^{\rm IB}$ are remarkably stable within the range of uncertainties of the measured slope parameters. Even if the latest experimental results that determine λ''_+ [29–32] do not agree perfectly with each other, all these results combined show a strong (anti)correlation between λ_+ and λ''_+ (see e.g. Fig. 8 in [32]). If we vary (λ_+, λ''_+) in the parameter space indicated by the different 1σ ellipses of [29–32], we find that $\mathcal{R}$ differs from $\mathcal{R}(1,0)$ by less than a per mille. With the present knowledge of the form factor $f_+(t)$, it is therefore already possible to predict $\mathcal{R}$ to excellent precision, and the biggest uncertainty (of the order of 0.4%) stems from unknown higher-order corrections in the structure dependent terms.

Table 5. Coefficients for the $\bar\lambda_+$, $\bar\lambda''_+$ dependence of $\mathcal{R}^{\rm IB}$, $\mathcal{R}$. The error margins for the $\mathcal{R}$ coefficients are due to uncertainties in higher-order contributions to the structure dependent terms

$\mathcal{R}^{\rm IB}(1,0)\cdot 10^2$	$c_1^{\rm IB}\cdot 10^3$	$c_2^{\rm IB}\cdot 10^4$	$c_3^{\rm IB}\cdot 10^4$
0.640	12.0	−5.4	16.6
$\mathcal{R}(1,0)\cdot 10^2$	$c_1\cdot 10^3$	$c_2\cdot 10^4$	$c_3\cdot 10^4$
0.633 ± 0.002	12.5 ± 0.4	-5.4 ± 0.3	16.9 ± 0.4

4.3 Dependence on the experimental cuts

We briefly study the dependence of the parameters in (38) on the experimental cuts by displaying their values for the alternative cuts $E_\gamma^{\rm cut} = 10\,{\rm MeV}$, $\theta_{e\gamma}^{\rm cut} = 10^\circ$ in Table 6. In addition, for historical reasons we also show results for the angle range $26^\circ \le \theta^*_{e\gamma} \le 53^\circ$ in combination with $E_\gamma^{\rm cut} = 10\,{\rm MeV}$; compare Table 1. $\mathcal{R}$ and $\mathcal{R}^{\rm IB}$ of course depend strongly on the cut values. The dependence on the form factor parameters, however, remains very mild also for these different cuts. In particular, the ratio $\mathcal{R}$ is even more stable with respect to variations of the form factor parameters, i.e. the variation of λ_+, λ''_+ in the range of the latest experimental results, as described above, leads to a change in $\mathcal{R}$ below the per mille level. As the difference between the coefficients c_i and $c_i^{\rm IB}$ is as small for all cuts as for the standard ones discussed in the previous subsection, we refrain from showing the $c_i^{\rm IB}$ in Table 6.

4.4 Isospin breaking and radiative corrections

As we can predict the ratio $\mathcal{R}$ to surprising precision of about half a percent, using Low's theorem, the experimentally available information on the K_{e3} form factor f_+, and ChPT for the structure dependent terms, we have to comment on isospin breaking corrections, generated by real and virtual photons and the light quark mass difference $m_u - m_d \neq 0$, which may clearly have an impact at the percent level.

As radiative corrections comprise the radiation of (additional) soft real photons, we have to specify the precise meaning of the ratio R as defined in (1), in the presence of virtual and real photons. We define the denominator to be the fully inclusive width $K^+ \to \pi^0 e^+ \nu_e(n\gamma)$, where $(n\gamma)$ denotes any number of photons of arbitrary energy. In analogy, the numerator in (1) refers to the measurement of radiative K^+_{e3} decays with at least one photon fulfilling the cut requirements $E^*_\gamma > E_\gamma^{\rm cut}$, $\theta^*_{e\gamma} > \theta_{e\gamma}^{\rm cut}$, plus arbitrary additional photons.

A complete calculation of radiative corrections in R is beyond the scope of this article. Below, we argue that the most

Table 6. $\mathcal{R}^{\rm IB}$, $\mathcal{R}$ for different values of the experimental cuts on $E_\gamma^{\rm cut}$, $\theta_{e\gamma}^{\rm cut}$, as well as coefficients for the $\bar\lambda_+$, $\bar\lambda''_+$ dependence of $\mathcal{R}$. The error margins for the $\mathcal{R}$ coefficients are due to uncertainties in higher-order contributions to the structure dependent terms

$E_\gamma^{\rm cut}$	$\theta_{e\gamma}^{\rm cut}$	$\mathcal{R}^{\rm IB}\cdot 10^2$	$\mathcal{R}\cdot 10^2$	$c_1\cdot 10^3$	$c_2\cdot 10^4$	$c_3\cdot 10^4$
30 MeV	20°	0.640	0.633 ± 0.002	12.5 ± 0.4	-5.4 ± 0.3	16.9 ± 0.4
30 MeV	10°	0.925	0.918 ± 0.002	11.1 ± 0.3	-4.7 ± 0.2	15.0 ± 0.3
10 MeV	20°	1.211	1.204 ± 0.002	7.5 ± 0.2	-3.2 ± 0.2	10.1 ± 0.2
10 MeV	10°	1.792	1.785 ± 0.002	6.7 ± 0.2	-2.8 ± 0.1	9.0 ± 0.1
10 MeV	26–53°	0.554	0.553 ± 0.001	5.7 ± 0.1	-2.4 ± 0.1	7.5 ± 0.1

Table 7. Coefficients for the K^+_{e3} phase space integral, including corrections of $\mathcal{O}(\alpha, m_u - m_d)$. The values for $a_{1,2}$ are taken from [34].[4] For a_0, see text

a_0	a_1	a_2	a_3	a_4
0.09583	0.3287	0.4535	3.124	6.136

sizeable effects can easily be taken care of, and that the unknown corrections can reasonably be expected to be small.

1. As was already argued in [20], the large short distance enhancement factor $S_{\rm EW} \propto \log M_Z/M_\rho$ that renormalized the Fermi coupling constant $G_{\rm F}$ [33–35] applies identically in numerator and denominator of R, so it cancels in the ratio.
2. In [34], isospin breaking corrections in K_{e3} were calculated in chiral perturbation theory up to and including $\mathcal{O}\big(p^2e^2, p^2(m_u - m_d)\big)$. Parts of these can be collected in a modified value for $f_+(0)$, which still cancels in R. In addition, the parameters a_i describing the slope parameter expansion of the K_{e3} phase space integral are shifted, the modified coefficients of the expanded phase space integral are given in Table 7. As in [34] the contribution of (single) real photon radiation was restricted to pion/electron momenta in agreement with non-radiative kinematics, we re-modify the coefficient a_0 to be fully inclusive again, increasing it by 0.51%.
3. The part of this estimate that is necessarily incomplete concerns isospin breaking corrections to the numerator of R. Radiative corrections that are potentially large are those enhanced by electron mass singularities. As we have defined the numerator of R to be *inclusive* with respect to additional photon radiation, such electron mass singularities should, according to the KLN theorem [36, 37], be taken care of by evaluating the running coupling constant at the scale of the kaon mass, $\alpha \to \alpha\big(1 + \frac{\alpha}{3\pi}\log(M_K^2/m_e^2)\big)$. In [34], a part of these large logarithms are absorbed into $f_+(0)$, which reduces the correction in the numerator to $\alpha \to \alpha\big(1 + \frac{\alpha}{12\pi}\log(M_K^2/m_e^2)\big)$.
4. We expect the remaining, non-enhanced, radiative corrections to be small, of the order of α/π. As a conservative estimate, we assign a relative uncertainty due to these of the size $\pm\Delta_{\rm em} = \pm 5\alpha/\pi \approx \pm 0.01$.
5. Finally, corrections in the numerator due to the light quark mass difference that are not local and absorbed in $f_+(0)$ are expected to be tiny and are neglected.

Summing everything up, we find that the corrections in the denominator of R plus the remaining electron mass logarithms enhance R by 1%. The estimated uncertainty in other radiative corrections is larger than that from higher-order chiral corrections in the structure dependent terms. Our combined predictions, for the various cut combinations discussed before, are summarized in Table 8.

We briefly compare the predictions in Table 8 to the experimental results shown in Table 1. We find very good agreement with [5] as well as with the standard cuts result in [8], while the values for R reported in [6, 7] as well as the one for the angular cut range 26–53° in [8] are a bit below the theoretical values, though disagreement hardly exceeds 1σ deviation. Clearly, forthcoming even more precise determinations of R [11, 12] are very welcome.

Table 8. Combined results for R for various cut combinations

$E_\gamma^{\rm cut}$	$\theta_{e\gamma}^{\rm cut}$	$R \cdot 10^2$
30 MeV	20°	0.640 ± 0.008
30 MeV	10°	0.928 ± 0.011
10 MeV	20°	1.217 ± 0.014
10 MeV	10°	1.804 ± 0.021
10 MeV	26–53°	0.559 ± 0.006

In [8], the ratio R is also given with no cut on $\theta^*_{e\gamma}$; see Table 1. It is difficult to provide a precise theoretical value of R for this situation, because the electron mass singularity renders the numerical integration over phase space unstable. While our calculation suggests a rather bigger value for R than what is quoted in Table 1, we refrain from working out a precise result. We do not, therefore, provide a final number in Table 8.

5 Structure dependent terms in differential rates

5.1 Photon energy distribution

It is obvious from the results of the previous section that a precise measurement of the ratio R is insufficient to determine structure dependent terms in $K^+_{e3\gamma}$: the shift in R is tiny and easily overwhelmed by the uncertainty in radiative corrections. It seems therefore more promising to use the more detailed experimental information contained in differential distributions for this purpose. In a pioneering study, the KTeV collaboration has attempted such an extraction of structure dependent contributions for $K^0_{e3\gamma}$ decays [13] by measuring the photon energy distribution, and their results were analyzed in detail in [20]. Here we provide the theoretical basis for such an analysis for $K^+_{e3\gamma}$, together with the chiral prediction for the outcome of such an extraction.

Among the various differential rates that may potentially be investigated, the one with respect to the photon energy E^*_γ is predestinated for a separation of bremsstrahlung and structure dependent terms, as the different behavior of both at small E^*_γ is the defining property to distinguish between the two contributions.

In the decomposition of the photon energy spectrum, we neglect terms that are proportional to structure dependent terms squared, and we use the working assumption discussed in Sect. 3 that the structure functions can reasonably well be approximated by constants. The photon

[4] We are grateful to V. Cirigliano for providing us with the numbers for $a_{3,4}$, which are not included in [34].

energy distribution thus reads

$$\frac{\mathrm{d}\Gamma}{\mathrm{d}E^*_\gamma} = \frac{\mathrm{d}\Gamma_{\mathrm{IB}}}{\mathrm{d}E^*_\gamma} + \sum_{i=1}^{4}\left(\langle V_i\rangle \frac{\mathrm{d}\Gamma_{V_i}}{\mathrm{d}E^*_\gamma} + \langle A_i\rangle \frac{\mathrm{d}\Gamma_{A_i}}{\mathrm{d}E^*_\gamma}\right) + \mathcal{O}\left(\left|T^{\mathrm{SD}}\right|^2, \Delta V_i, \Delta A_i\right) . \quad (39)$$

Here $\mathrm{d}\Gamma_{V_i}/\mathrm{d}E^*_\gamma$ is defined to be the part of the spectrum proportional to V_i, etc., and ΔV_i, ΔA_i stand for the errors made by the approximation of constant structure functions.

We remind the reader that V_3, A_3 are suppressed by m_e^2/M_K^2 and are therefore essentially unobservable. Furthermore, we find that the distributions $\mathrm{d}\Gamma_{V_4}/\mathrm{d}E^*_\gamma$, $\mathrm{d}\Gamma_{A_4}/\mathrm{d}E^*_\gamma$ are considerably smaller than the other structure dependent parts of the spectrum; adding to that the observation that $\langle V_4\rangle$, $\langle A_4\rangle$ are suppressed by two orders in the chiral expansion with respect to $\langle V_{1,2}\rangle$, $\langle A_{1,2}\rangle$, we neglect these structures and only discuss the effects of $V_{1,2}$, $A_{1,2}$ for simplicity reasons.

The remaining parts of the photon spectrum $\mathrm{d}\Gamma_X/\mathrm{d}E^*_\gamma$ are shown in Fig. 2. Note that in order to put all spectra in one plot, the bremsstrahlung spectrum has been scaled down by two orders of magnitude. While $\mathrm{d}\Gamma_{\mathrm{IB}}/\mathrm{d}E^*_\gamma$ displays the expected $1/E^*_\gamma$ singularity for small photon energies, the structure dependent parts $\mathrm{d}\Gamma_X/\mathrm{d}E^*_\gamma$ with $X = V_1$, V_2, A_1 perturb the pure bremsstrahlung spectrum all essentially in the same way: they rise linearly with E^*_γ for small energies, are bent down by phase space at maximum photon energies, and display a maximum between 80 MeV and 100 MeV. Even though the strength of the perturbation varies, the shape is nearly the same for all three. Only the distribution $\mathrm{d}\Gamma_{A_2}/\mathrm{d}E^*_\gamma$ has an additional node in between and is therefore suppressed.

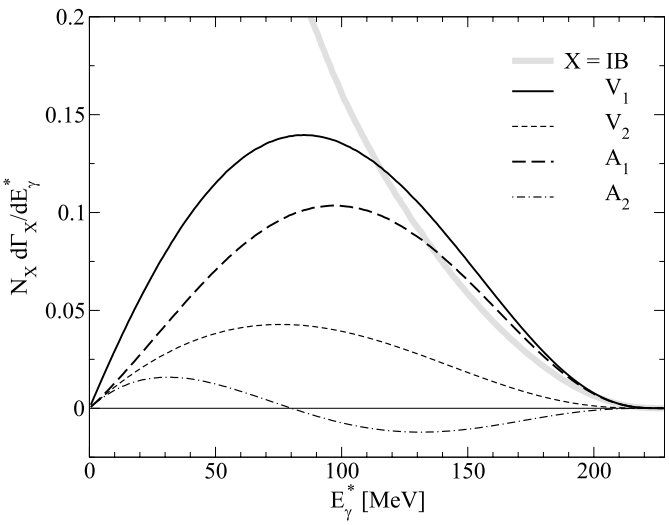

Fig. 2. Photon energy distributions from inner bremsstrahlung as well as the various structure dependent terms. The notation $\mathrm{d}\Gamma_X/\mathrm{d}E^*_\gamma$ for the various X refers to (39). The normalization factors are $N_{V_i,\,A_i} = 100\,N_{\mathrm{IB}} = 10^3 M_K/\Gamma(K_{e3})$. We only cut on the electron–photon angle, $\theta^{\mathrm{cut}}_{e\gamma} = 20^\circ$

Similarly to the neutral kaon decay channel [20], we find that the bremsstrahlung spectrum is perturbed by a function $f(E^*_\gamma)$, where

$$f(E^*_\gamma) \doteq \frac{\mathrm{d}\Gamma_{V_1}}{\mathrm{d}E^*_\gamma} \approx 3.3 \times \frac{\mathrm{d}\Gamma_{V_2}}{\mathrm{d}E^*_\gamma} \approx 1.3 \times \frac{\mathrm{d}\Gamma_{A_1}}{\mathrm{d}E^*_\gamma} . \quad (40)$$

The information on the SD terms is contained in the effective strength $\langle X\rangle$ that multiplies $f(E^*_\gamma)$,

$$\frac{\mathrm{d}\Gamma}{\mathrm{d}E^*_\gamma} \approx \frac{\mathrm{d}\Gamma_{\mathrm{IB}}}{\mathrm{d}E^*_\gamma} + \langle X\rangle\, f(E^*_\gamma) ,$$
$$\langle X\rangle = \langle V_1\rangle + 0.3\,\langle V_2\rangle + 0.7\,\langle A_1\rangle . \quad (41)$$

Taking into account the chiral predictions for the various averaged structure functions, see Table 2, we find that $\langle X\rangle$ is dominated by $\langle V_1\rangle$ and $\langle A_1\rangle$, both of which contribute with comparable strength. Corrections from $\langle V_2\rangle$, $\langle A_2\rangle$ are suppressed effectively by roughly a factor of 20. Numerically, we predict the effective strength $\langle X\rangle$ to be

$$\langle X\rangle = \begin{cases} -2.2 & \mathcal{O}(p^4) , \\ -2.2 \pm 0.7 & \mathcal{O}(p^6) . \end{cases} \quad (42)$$

We therefore conclude that a significant part of the structure dependent photon spectrum is due to the chiral anomaly (A_1). This is different from the decay $K^0_{e3\gamma}$ [20], where A_1 vanishes at $\mathcal{O}(p^4)$, and the contribution of A_2 to the photon spectrum is comparably suppressed as in Fig. 2. The importance of the chiral anomaly for the existence of various contributions to T-odd correlations in $K^+_{e3\gamma}$ was emphasized in [23], therefore it plays a significant role in the phenomenology of this process.

5.2 Other distributions

It is particularly interesting to trace back effects of the chiral anomaly even more clearly; i.e., we would like to separate the contributions of V_1 and A_1 that can only be measured as a (weighted) sum in the photon energy distribution. This turns out to be rather difficult: in many differential distributions, both are practically indistinguishable from each other and/or from the dominant bremsstrahlung spectrum. Two notable exceptions are shown in Fig. 3: the distributions with respect to the (cosines of) the angles between electron and pion, as well as between neutrino and photon, show strongly different behavior in backward directions for the parts of the spectra proportional to $\langle V_1\rangle$ and $\langle A_1\rangle$. In particular, $\mathrm{d}\Gamma_{A_1}/\mathrm{d}\cos\theta^*_{e\pi}$ and $\mathrm{d}\Gamma_{A_1}/\mathrm{d}\cos\theta^*_{\nu\gamma}$ go through zero here.

A strategy for an advanced study of structure dependent terms that tries to disentangle the two most important SD contributions $\langle V_1\rangle$ and $\langle A_1\rangle$ on purely experimental grounds, without input from ChPT, might therefore proceed along the following lines:

1. determine the effective strength $\langle X\rangle \approx \langle V_1\rangle + 0.7\langle A_1\rangle$ from an analysis of the photon energy spectrum;
2. use this constraint for an additional fit to the angular spectra $\mathrm{d}\Gamma/\mathrm{d}\cos\theta^*_{e\pi}$ and/or $\mathrm{d}\Gamma/\mathrm{d}\cos\theta^*_{\nu\gamma}$ in order to determine $\langle V_1\rangle$ and $\langle A_1\rangle$ separately.

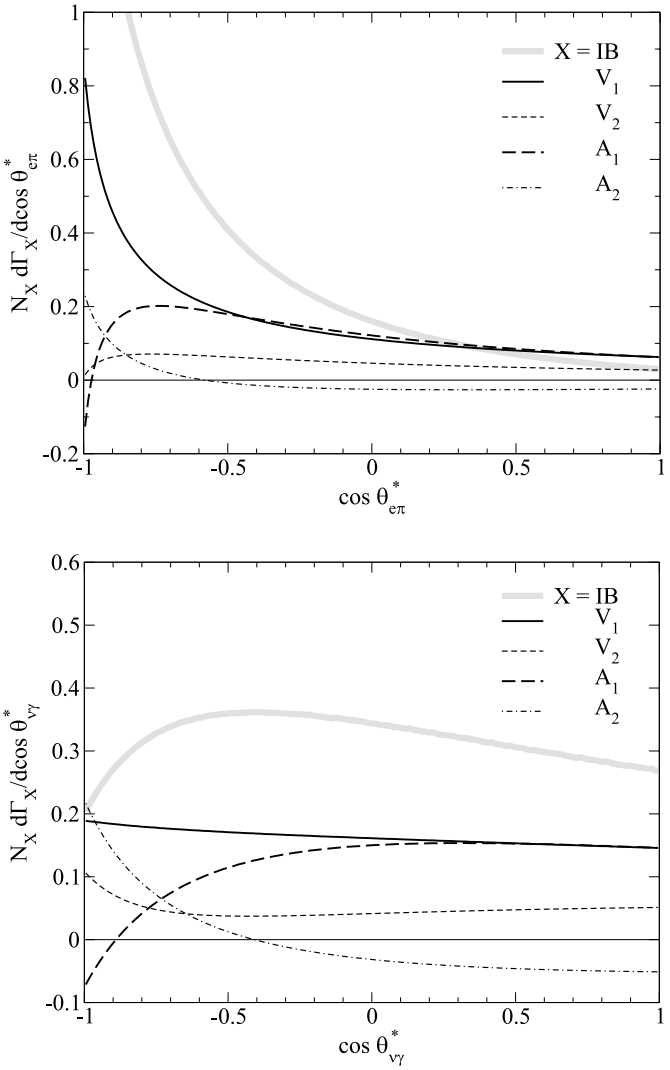

Fig. 3. Distributions with respect to $\cos\theta^*_{e\pi}$, $\cos\theta^*_{\nu\gamma}$ from inner bremsstrahlung as well as the various structure dependent terms. The notation $\mathrm{d}\Gamma_X/\mathrm{d}\cos\theta^*_{e\pi}$, $\mathrm{d}\Gamma_X/\mathrm{d}\cos\theta^*_{\nu\gamma}$, is chosen in analogy to (39). The normalization factors are $N_{V_i,\,A_i} = 100\,N_{\mathrm{IB}} = 10^4/\Gamma(K_{e3})$. Both spectra are shown for the standard cuts $E_\gamma^{\mathrm{cut}} = 30\,\mathrm{MeV}$, $\theta_{e\gamma}^{\mathrm{cut}} = 20^\circ$

The (numerically) subleading structure functions $\langle V_2\rangle$, $\langle A_2\rangle$ are, due to their smallness, even more difficult to determine. In principle, one finds a similar picture for these as in the case of $K^0_{e3\gamma}$ [20]: the distribution $\mathrm{d}\Gamma_{V_2}/\mathrm{d}E^*_\pi$ peaks at lower pion energies than bremsstrahlung and the dominant structure dependent terms, and $\mathrm{d}\Gamma_{A_2}/\mathrm{d}\cos\theta^*_{e\gamma}$ produces a slightly enhanced variation in backward directions. However, these effects are expected to be much harder to measure even than the structure dependent modification of the photon energy spectrum.

We want to briefly comment on the differential distributions $\mathrm{d}\Gamma/\mathrm{d}\cos\theta^*_{e\gamma}$, the different contributions to which are displayed in Fig. 4. [Note again that the bremsstrahlung contribution is scaled down by two orders of magnitude with respect to the structure dependent ones.] In [8], a discrepancy between data and Monte Carlo was found for

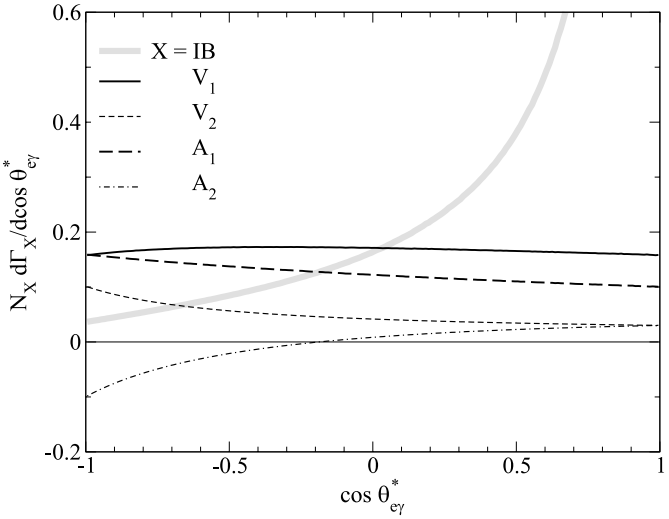

Fig. 4. Distributions with respect to $\cos\theta^*_{e\gamma}$ from inner bremsstrahlung as well as the various structure dependent terms. The notation $\mathrm{d}\Gamma_X/\mathrm{d}\cos\theta^*_{e\gamma}$ is chosen in analogy to (39). The normalization factors are $N_{V_i,\,A_i} = 100\,N_{\mathrm{IB}} = 10^4/\Gamma(K_{e3})$. The photon energy cut $E_\gamma^{\mathrm{cut}} = 30\,\mathrm{MeV}$ was applied

$\cos\theta^*_{e\gamma} \approx -1$, and the authors comment that this "could possibly be interpreted as a direct emission effect". It is obvious from Fig. 4 that ChPT makes this claim untenable: the effects of structure dependent terms are too small and in particular far too flat in their angular distributions to produce a visible peak as seen in Fig. 8 of [8]. The resulting total curve IB + SD would still lie within the width of the grey line for the IB contribution shown in Fig. 4.

6 Conclusions

In this article, we have analyzed various aspects of $K^+_{e3\gamma}$ decays, spinning forth previous work on $K^0_{e3\gamma}$. Our findings can be summarized as follows.

1. We have constructed a decomposition of the $K^+_{e3\gamma}$ decay amplitude into an inner bremsstrahlung and a structure dependent part, in the absence of radiative corrections, that guarantees that the SD part has no non-trivial analytic properties except for unitarity cuts.
2. By applying this decomposition to the chiral representation of the $K^+_{\ell 3\gamma}$ amplitude of order p^4 [18], we derive the leading chiral predictions for the structure functions. The axial structure functions that are given in terms of the Wess–Zumino–Witten anomaly are constant, while the vector structure functions, although given in terms of complicated loop functions, are shown to be free of cuts in the physical region and therefore smooth and very close to constant.
3. We consider higher-order corrections of order p^6 to the structure functions, in particular, we present the complete order p^6 expressions for the axial terms. Although cuts in the physical region due to intermediate two-

pion states appear, their cusp behavior is shown to be of P-wave type and therefore suppressed, such that the real parts of the A_i are still smooth to a reasonable approximation. The size of (incomplete) higher-order polynomial corrections to the vector structure functions is estimated to be of natural size for chiral $SU(3)$ corrections.

4. We have investigated the stability of the prediction of the relative branching ratio R, normalized to the non-radiative width, with respect to K_{e3} form factor parameters. Within the range of uncertainty of the available experimental information on these parameters, R is shown to be remarkably stable at the per mille level. Structure dependent terms reduce R by about 1%. Our combined prediction for experimental cuts of $E_\gamma^{\rm cut} = 30\,\mathrm{MeV}$, $\theta_{e\gamma}^{\rm cut} = 20^\circ$ is

$$R = (0.640 \pm 0.008) \times 10^{-2}\,, \tag{43}$$

where the uncertainty is dominated by unknown radiative corrections. Predictions for other cut values were also given in Table 6.

5. We have discussed how to extract a linear combination of structure dependent terms from an experimental analysis of the differential rate $\mathrm{d}\Gamma/\mathrm{d}E_\gamma^*$. In contrast to $K^0_{e3\gamma}$, the axial anomaly contributes significantly to the perturbation of the bremsstrahlung spectrum, such that effects may actually be visible in $K^+_{e3\gamma}$. As a second step, we have pointed out that angular distributions of the type $\mathrm{d}\Gamma/\mathrm{d}\cos\theta^*_{e\pi}$ and/or $\mathrm{d}\Gamma/\mathrm{d}\cos\theta^*_{\nu\gamma}$ may allow for a disentanglement of the two dominant structure dependent terms V_1 and A_1.

It would be extremely interesting and rewarding to see the various predictions tested by the modern high-statistics kaon decay experiments such as NA48/2 [11] or KEK-E470 [12], in particular to find unambiguous signals for the physics behind the structure dependent terms.

Note added in proof

After submission of this article for publication, an updated and substantially revised version of the ISTRA experiment appeared [8]. Several of the results of these authors discussed here have undergone a change; in particular the differences with our predictions concerning some of the results on R and on the angular distribution with respect to $\cos\theta^*_{e\gamma}$ have disappeared.

Acknowledgements. We thank Nello Paver and Michela Verbeni for collaboration in an early stage of this project. We are grateful to Stefano Venditti for useful communications. This work was supported in parts by the EU Integrated Infrastructure Initiative Hadron Physics Project (contract number RII3–CT–2004–506078), by DFG (SFB/TR 16, "Subnuclear Structure of Matter"), by the Swiss National Science Foundation, by RTN, BBW-Contract No. 01.0357, and EC-Contract HPRN-CT2002-00311 (EURIDICE). J.G. is grateful to the Alexander von Humboldt-Stiftung and to the Helmholtz-Gemeinschaft for a grant, and he thanks the HISKP, where part of this work was performed, for the warm hospitality. E.H.M. thanks the "Studienstiftung des deutschen Volkes" for supporting his studies.

Appendix A: Inner bremsstrahlung in $K^+_{e3\gamma}$ decays

In this appendix we discuss the separation of the hadronic tensor $V_{\mu\nu}$ into an IB and a SD part. The relevant diagrams can be grouped in two classes, displayed in Fig. 5. The hatched blobs denote one-particle irreducible contributions. The diagram b) generates a pole in the variable $u = (p-q)^2$, at $u = M_K^2$, corresponding to the intermediate K^+ state. We isolate the contribution of this pole by writing

$$V_{\mu\nu} = \widetilde{V}_{\mu\nu} + \frac{1}{\sqrt{2}}\frac{p_\mu}{pq}\left[2p'_\nu f_+\left(W^2\right) + W_\nu f_1\left(W^2\right)\right]\,, \tag{A.1}$$

where $W = p - p' - q$. In the following, we assume that this is the only singular part at $q = 0$ in the tensor $V_{\mu\nu}$, or, in other words, that $\widetilde{V}_{\mu\nu}$ is regular at $q = 0$. This is the only assumption in the derivation of the final expression for the IB term. We have checked that it is true at one-loop order in ChPT, and we see no reason why it should not be correct to any order and thus be true in QCD.

We write this regular part as

$$\begin{aligned}\widetilde{V}_{\mu\nu} = \frac{1}{\sqrt{2}}\big[&v_0\, g_{\mu\nu} + v_1\, p'_\mu q_\nu + v_2\, W_\mu q_\nu + v_3\, p'_\mu W_\nu \\ &+ v_4\, p'_\mu p'_\nu + v_5\, W_\mu p'_\nu + v_6\, W_\mu W_\nu\big]\,.\end{aligned} \tag{A.2}$$

The Ward identity (7) generates three conditions on $\widetilde{V}_{\mu\nu}$ that can be written as

$$\begin{aligned} v_0 + v_1\, p'q + v_2\, qW &= f_1\,, \\ v_3\, p'q + v_6\, qW &= \Delta f_1\,, \\ v_4\, p'q + v_5\, qW &= 2\Delta f_+\,, \end{aligned} \tag{A.3}$$

with

$$\Delta f_i = f_i(t) - f_i\left(W^2\right)\,, \quad i = +, 1\,. \tag{A.4}$$

The first equation can be solved for v_0. Furthermore, we set

$$v_5 = \frac{2\Delta f_+}{qW} + \tilde{v}_5\,,\ v_6 = \frac{\Delta f_1}{qW} + \tilde{v}_6\,. \tag{A.5}$$

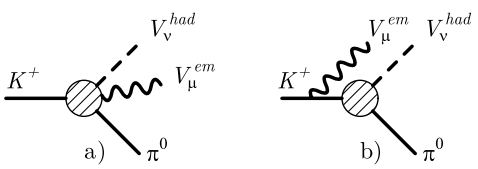

Fig. 5. Diagrams for $V_{\mu\nu}$, evaluated in the framework of ChPT. The hatched blobs denote one-particle irreducible graphs

and find

$$v_4\, p'q + \tilde{v}_5\, qW = 0\,,$$
$$v_3\, p'q + \tilde{v}_6\, qW = 0\,. \tag{A.6}$$

We use the fact that the Lorentz invariant amplitudes v_i are defined for any value of the kinematic variables $p'q$, qW, and that the amplitudes are assumed to be non-singular at $p'q = 0$. It then follows that $\tilde{v}_{5,6}$ are proportional to $p'q$,

$$\tilde{v}_{5,6} = -p'q\, \tilde{v}_{4,3}\,, \tag{A.7}$$

where the sign and the numbering is chosen for convenience. Finally, we obtain

$$v_{3,4} = qW\, \tilde{v}_{3,4}\,. \tag{A.8}$$

Collecting the results, we find that $V^{\rm SD}_{\mu\nu}$ can be written in the form displayed in (15), with

$$(V_1, V_2, V_3, V_4) = (v_1, v_2, \tilde{v}_3, \tilde{v}_4)\,. \tag{A.9}$$

Equation (26) contains the explicit expression of the form factors V_i in the limit $q = 0$, $t = 0$, illustrating that they indeed are non-singular at $q = 0$ at next-to-leading order in ChPT, as mentioned above.

Appendix B: Traces

Here, we give the explicit expression for the sum over spins in $|T|^2$ in the limit where the relevant traces are evaluated at $m_e = 0$. We write

$$\begin{aligned} N^{-1} \sum_{\rm spins} |T|^2 = {} & a_1\, f_+(t)^2 + a_2\, f_+(t) \delta f_+ + a_3\, \delta f_+^2 \\ & + \sum_{i=1}^{4} \Big[\big(b_i\ {\rm Re}\, V_i + b_i^5\ {\rm Re}\, A_i\big) f_+(t) \\ & \qquad + \big(c_i\ {\rm Re}\, V_i + c_i^5\ {\rm Re}\, A_i\big) \delta f_+ \Big] \\ & + \mathcal{O}\big({\rm Im} V_i, {\rm Im} A_i, V_i^2, A_i^2, V_i A_i\big)\,, \end{aligned} \tag{B.1}$$

with

$$\delta f_+ = M_K^2 (qW)^{-1} \left[f_+(t) - f_+\left(W^2\right) \right]\,,$$
$$N = 8\pi\alpha G_{\rm F}^2 |V_{us}|^2 M_K^2\,. \tag{B.2}$$

For the neglected terms proportional to imaginary parts in the structure functions V_i, A_i, see [23]. With this convention for N, the right hand side in (B.1) is dimensionless. In the limit $m_e = 0$, we immediately have

$$b_3 = b_3^5 = c_3 = c_3^5 = 0\,. \tag{B.3}$$

We use the abbreviations

$$\begin{aligned} & z\, pp' = a\,,\ z\, pq = b\,,\ z\, pp_e = c\,,\ z\, pp_\nu = d\,, \\ & z\, p'q = e\,,\ z\, p'p_e = f\,,\ z\, p'p_\nu = g\,,\ z\, p_e q = h\,, \\ & z\, p_\nu q = j\,,\ z\, p_e p_\nu = k\,,\ z\, pW = l\,,\ z\, p'W = m\,, \\ & z\, qW = n\,,\ z\, M_\pi^2 = r\,,\ z\, = M_K^{-2}\,, \end{aligned} \tag{B.4}$$

Table 9. Prefactors that multiply the $\bar{a}_i$, $\bar{b}_i$ etc.

$\hat{a}_1$	$4/\big(b^2 h\big)$	$\hat{b}_1$	$4/\big(bhz\big)$	$\hat{b}_1^5$	$4/\big(bhz\big)$
$\hat{a}_2$	$4/\big(b^2 h\big)$	$\hat{b}_2$	$4/\big(bhz\big)$	$\hat{b}_2^5$	$4/\big(bhz\big)$
$\hat{a}_3$	$4/b^2$	$\hat{b}_4$	$2/\big(bhz^2\big)$	$\hat{b}_4^5$	$2/\big(hz^2\big)$
		$\hat{c}_1$	$4/\big(bz\big)$	$\hat{c}_1^5$	$4/\big(bz\big)$
		$\hat{c}_2$	$4/\big(bz\big)$	$\hat{c}_2^5$	$4n/\big(bz\big)$
		$\hat{c}_4$	$4/\big(bz^2\big)$	$\hat{c}_4^5$	$1/z^2$

and decompose all the coefficients according to $a_i = \hat{a}_i\, \bar{a}_i$ etc., where the prefactors $\hat{a}_i$, $\hat{b}_i$ ... are collected in Table 9.

We obtain the following expressions for the coefficients $\bar{a}_i$, $\bar{b}_i$ and so on:

$$\begin{aligned} \bar{a}_1 = {} & -2\,a\,b\,g\,h + 2\,b^2 f\,g + 2\,b^2 g\,e - b^2 j\,r \\ & - b^2 k\,r + 4\,b\,c\,f\,g + 2\,b\,c\,g\,e - b\,c\,j\,r \\ & - 2\,b\,c\,k\,r + b\,d\,h\,r - 2\,f\,g\,h + h\,k\,r\,, \\ \bar{a}_2 = {} & 2\,a\,b\,g\,h\,n + 4\,b^2 f\,g\,k - 2\,b^2 g\,h\,m + 2\,b^2 g\,k\,e \\ & + b^2 h\,k\,r - b^2 j\,k\,r - 2\,b^2 k^2 r - 4\,b\,c\,f\,g\,n \\ & - 2\,b\,c\,g\,n\,e + b\,c\,j\,n\,r + 2\,b\,c\,k\,n\,r - b\,d\,h\,n\,r \\ & - 4\,b\,f\,g\,h\,l + 2\,b\,h\,k\,l\,r + 4\,f\,g\,h\,n - 2\,h\,k\,n\,r\,, \\ \bar{a}_3 = {} & -4\,b^2 f\,g\,k + 2\,b^2 k^2 r + 4\,b\,f\,g\,l\,n \\ & - 2\,b\,k\,l\,n\,r - 2\,f\,g\,n^2 + k\,n^2 r\,, \\ \bar{b}_1 = {} & -a\,f\,h\,j - a\,g\,h^2 + b\,f^2 j + b\,f\,g\,h - b\,f\,k\,e \\ & + 2\,b\,g\,h\,e - b\,h\,j\,r + c\,g\,h\,e + d\,f\,h\,e\,, \\ \bar{b}_2 = {} & -a\,h\,k\,n + b\,f\,j\,k + b\,g\,h\,k + b\,g\,h\,n \\ & - b\,h\,j\,m + b\,h\,k\,e - b\,k^2 e + c\,g\,h\,n \\ & + d\,f\,h\,n - f\,h\,j\,l - g\,h^2 l + h\,k\,l\,e\,, \\ \bar{b}_4 = {} & -4\,a\,f\,g\,h\,n + 2\,a\,h\,k\,n\,r + 4\,b\,f^2 g\,n - 4\,b\,f\,g\,k\,e \\ & + 2\,b\,f\,g\,n\,e - b\,f\,j\,n\,r - 2\,b\,f\,k\,n\,r + 2\,b\,g\,h\,m\,e \\ & - b\,g\,h\,n\,r - 2\,b\,g\,k\,e^2 - b\,h\,k\,r\,e + b\,j\,k\,r\,e \\ & + 2\,b\,k^2 r\,e + 4\,f\,g\,h\,l\,e - 2\,h\,k\,l\,r\,e\,, \\ \bar{b}_1^5 = {} & a\,f\,h\,j - a\,g\,h^2 - b\,f^2 j + b\,f\,g\,h + b\,f\,k\,e + 2\,b\,g\,h\,e \\ & - b\,h\,j\,r - b\,h\,k\,r + c\,g\,h\,e - c\,h\,j\,r - d\,f\,h\,e + d\,h^2 r\,, \\ \bar{b}_2^5 = {} & a\,h^2 k - a\,h\,j\,k - b\,f\,h\,k + b\,f\,j\,k - b\,g\,h\,n \\ & + b\,h\,j\,m + b\,h\,k\,m - b\,h\,k\,e - b\,k^2 e + c\,h\,j\,m \\ & - c\,h\,k\,e - d\,h^2 m + d\,h\,k\,e\,, \\ \bar{b}_4^5 = {} & 2\,f\,g\,n\,e - f\,j\,n\,r + 2\,g\,h\,m\,e - g\,h\,n\,r \\ & - 2\,g\,k\,e^2 - h\,k\,r\,e + j\,k\,r\,e\,, \\ \bar{c}_1 = {} & a\,f\,j\,n + a\,g\,h\,n - b\,f\,j\,m + b\,f\,k\,e \\ & - b\,g\,h\,m + b\,g\,k\,e - c\,g\,n\,e - d\,f\,n\,e\,, \\ \bar{c}_2 = {} & a\,k\,n^2 - 2\,b\,f\,j\,k + b\,f\,k\,n - 2\,b\,g\,h\,k \\ & + b\,g\,k\,n + 2\,b\,k^2 e - b\,k\,m\,n - c\,g\,n^2 \\ & - d\,f\,n^2 + f\,j\,l\,n + g\,h\,l\,n - k\,l\,n\,e\,, \\ \bar{c}_4 = {} & 2\,a\,f\,g\,n^2 - a\,k\,n^2 r + 4\,b\,f\,g\,k\,e - 2\,b\,f\,g\,m\,n \\ & - 2\,b\,k^2 r\,e + b\,k\,m\,n\,r - 2\,f\,g\,l\,n\,e + k\,l\,n\,r\,e\,, \end{aligned}$$

$$
\begin{aligned}
\bar{c}_1^5 &= -a\,f\,j\,n + a\,g\,h\,n + b\,f\,j\,m - b\,f\,k\,e \\
&\quad - b\,g\,h\,m + b\,g\,k\,e + b\,h\,k\,r - b\,j\,k\,r \\
&\quad - c\,g\,n\,e + c\,j\,n\,r + d\,f\,n\,e - d\,h\,n\,r\,, \\
\bar{c}_2^5 &= -a\,h\,k + a\,j\,k - c\,j\,m + c\,k\,e + d\,h\,m - d\,k\,e\,, \\
\bar{c}_4^5 &= 0\,. \qquad \text{(B.5)}
\end{aligned}
$$

Appendix C: Axial form factors at order p^6

In this appendix, we give the explicit formulae for the next-to-leading order corrections to the axial form factors A_1, A_2, and A_4, as written out formally in (27). The necessary loop diagrams for this calculation are displayed in Fig. 6. We find the following combinations of loop functions and counterterms:

$$
\begin{aligned}
S_1(s) &= H_{\pi\pi}(s) + 3H_{KK}(s) + \frac{16\pi^2}{3}\,C^{\mathrm{r}}_{1s}\,s\,, \\
S_2(s) &= \frac{16\pi^2}{3}\,C_{2s}\,s\,, \\
T_1(t) &= \frac{1}{2}H_{K\pi}(t) + \frac{1}{2}H_{\eta K}(t) + \frac{16\pi^2}{3}\,C^{\mathrm{r}}_{1t}\,t\,, \\
T_2(t) &= T_{K\pi}(t) - T_{\eta K}(t) + \frac{16\pi^2}{3}\,C^{\mathrm{r}}_{2t}\,t\,, \\
U_1(u) &= \frac{1}{2}H_{K\pi}(u) + \frac{1}{2}H_{\eta K}(u) + \frac{16\pi^2}{3}\,C^{\mathrm{r}}_{1u}\,u\,, \\
U_2(u) &= 2H_{K\pi}(u) + 2H_{\eta K}(u) + \frac{16\pi^2}{3}\,C^{\mathrm{r}}_{2u}\,u\,, \\
X_1 &= 2\mu_\pi - \mu_K - \mu_\eta + \frac{16\pi^2}{3}\big(C^{\mathrm{r}}_{1\pi}M_\pi^2 + C^{\mathrm{r}}_{1K}M_K^2\big)\,,
\end{aligned}
$$

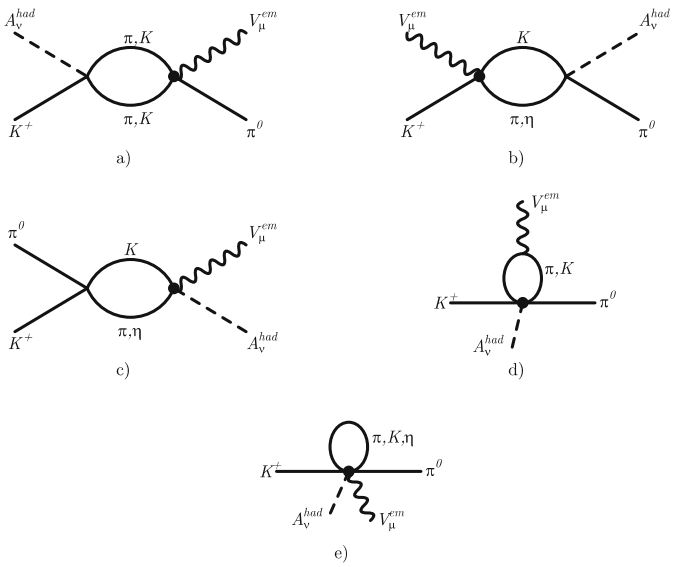

Fig. 6. Diagrams that contribute to the anomalous amplitude $A_{\mu\nu}$ at order p^6 [in a), the contribution from π, η intermediate states vanishes]. Charges of the mesons running in the loops are not indicated. The filled vertices denote a contribution from the anomalous Lagrangian at order p^4. External line insertions in the tree diagram of order p^4 are not displayed

$$
\begin{aligned}
X_2 &= \frac{19}{12}\mu_\pi - \frac{19}{6}\mu_K + \frac{1}{4}\mu_\eta \\
&\quad + \frac{16\pi^2}{3}\big(C^{\mathrm{r}}_{2\pi}M_\pi^2 + C^{\mathrm{r}}_{1K}M_K^2\big)\,. \qquad \text{(C.1)}
\end{aligned}
$$

The loop function $H_{ab}(x)$ is given by

$$
\begin{aligned}
H^{\mathrm{r}}_{ab}(x) &= \frac{1}{12F^2}\Bigg\{\frac{\lambda\left(x, M_a^2, M_b^2\right)}{x}\,\bar{J}_{ab}(x) + \frac{x - 3\Sigma_{ab}}{24\pi^2} \qquad \text{(C.2)} \\
&\quad - \frac{x}{32\pi^2}\log\frac{M_a^2 M_b^2}{\mu^4} - \frac{x\,\Sigma_{ab} - 8M_a^2M_b^2}{32\pi^2\Delta_{ab}}\log\frac{M_a^2}{M_b^2}\Bigg\},
\end{aligned}
$$

where the loop function $\bar{J}_{ab}(x)$ is defined according to

$$
\begin{aligned}
\bar{J}_{ab}(t) &= J_{ab}(t) - J_{ab}(0)\,, \\
J_{ab}(q^2) &= \frac{1}{\mathrm{i}}\int\frac{\mathrm{d}^d l}{(2\pi)^d}\,\frac{1}{\left(M_a^2 - l^2\right)\left(M_b^2 - (l-q)^2\right)}\,. \qquad \text{(C.3)}
\end{aligned}
$$

The other functions can also be written in relatively compact forms:

$$
\begin{aligned}
T^{\mathrm{r}}_{K\pi}(t) &= -\frac{1}{24F^2}\Bigg\{13t\Bigg[\bar{J}_{K\pi}(t) \\
&\quad - \frac{1}{32\pi^2}\left(\log\frac{M_K^2M_\pi^2}{\mu^4} + \frac{\Sigma_{K\pi}}{\Delta_{K\pi}}\log\frac{M_K^2}{M_\pi^2}\right)\Bigg] \\
&\quad - \Bigg[2\Sigma_{K\pi} - 8\Delta_{K\pi} \\
&\quad + \left(16\Sigma_{K\pi} + 11\Delta_{K\pi} - \frac{8\Delta_{K\pi}^2}{t}\right)\frac{\Delta_{K\pi}}{t}\Bigg]\bar{J}_{K\pi}(t) \\
&\quad + \frac{M_K^2M_\pi^2(2\Delta_{K\pi} + t)}{4\pi^2 t\Delta_{K\pi}}\log\frac{M_K^2}{M_\pi^2} \\
&\quad - \frac{(t - 3\Sigma_{K\pi})(t - \Delta_{K\pi})}{12\pi^2 t}\Bigg\}\,, \qquad \text{(C.4)} \\
T^{\mathrm{r}}_{\eta K}(t) &= \frac{1}{24F^2}\Bigg\{t\Bigg[\bar{J}_{\eta K}(t) \\
&\quad - \frac{1}{32\pi^2}\left(\log\frac{M_\eta^2M_K^2}{\mu^4} + \frac{\Sigma_{\eta K}}{\Delta_{\eta K}}\log\frac{M_\eta^2}{M_K^2}\right)\Bigg] \\
&\quad + \Bigg[2\Sigma_{\eta K} + 8\Delta_{\eta K} \\
&\quad - \left(\frac{8}{3}\Sigma_{\eta K} + 9\Delta_{\eta K} - \frac{8\Delta_{\eta K}^2}{t}\right)\frac{\Delta_{K\pi}}{t}\Bigg]\bar{J}_{\eta K}(t) \\
&\quad + \frac{M_\eta^2M_K^2(2\Delta_{K\pi} - t)}{4\pi^2 t\Delta_{\eta K}}\log\frac{M_\eta^2}{M_K^2} \\
&\quad - \frac{(t - 3\Sigma_{\eta K})(t - \Delta_{K\pi})}{12\pi^2 t}\Bigg\}\,, \qquad \text{(C.5)} \\
\mu_a &= \frac{M_a^2}{32\pi^2F^2}\log\frac{M_a^2}{\mu^2}\,, \qquad \text{(C.6)}
\end{aligned}
$$

where we have used $\Sigma_{ab} = M_a^2 + M_b^2$, $\Delta_{ab} = M_a^2 - M_b^2$, and the two point function $\bar{J}_{ab}(x)$ as defined in (C.3). The combinations of low-energy constants occurring in (27) and

Table 10. The coefficients from (C.1) in terms of the renormalized low-energy constants $C_i^{W\mathrm{r}}$. For example, $C^{\mathrm{r}}_{1s} = -C^{W\mathrm{r}}_{13} - 5C^{W\mathrm{r}}_{14} + \cdots$. Constants without superscript r are scale independent

	C^{r}_{1s}	C^{r}_{1t}	C^{r}_{1u}	$C^{\mathrm{r}}_{1\pi}$	C^{r}_{1K}	C_{2s}	C^{r}_{2t}	C^{r}_{2u}	$C^{\mathrm{r}}_{2\pi}$	C^{r}_{2K}	C_{4A}
$C^{W\mathrm{r}}_2$	0	0	0	24	−24	0	0	0	0	0	0
$C^{W\mathrm{r}}_4$	0	0	0	16	4	0	0	0	64	0	0
$C^{W\mathrm{r}}_5$	0	0	0	−4	8	0	0	0	−16	0	0
C^{W}_7	0	0	0	0	0	0	0	0	64	−16	0
C^{W}_9	0	0	0	0	0	0	0	0	−48	0	0
$C^{W\mathrm{r}}_{11}$	0	0	0	0	0	0	0	0	96	−48	0
$C^{W\mathrm{r}}_{13}$	−1	−4	−1	−2	4	−4	−2	0	−22	2	−16
$C^{W\mathrm{r}}_{14}$	−5	7	−2	−6	−3	−20	8	0	−4	−8	48
$C^{W\mathrm{r}}_{15}$	4	−2	4	−6	−6	16	8	0	−40	−8	−32
$C^{W\mathrm{r}}_{19}$	1	1	1	−1	−1	4	2	0	−2	−2	0
$C^{W\mathrm{r}}_{20}$	−1	−1	−4	4	1	−4	−8	0	20	8	16
$C^{W\mathrm{r}}_{21}$	−4	−4	−4	4	4	−16	−8	0	8	8	0
$C^{W\mathrm{r}}_{22}$	5/2	5/2	1	−1	−5/2	−6	2	4	4	−2	8
C^{W}_{23}	−9/2	−9/2	−6	6	9/2	−6	−6	0	12	6	8

(C.1) are given in Table 10 according to the numbering in [38].

Appendix D: Numerical parameters

We denote the neutral pion and charged kaon masses with M_π and M_K, respectively. In numerical evaluations, we use

$$\begin{aligned} M_K &= 493.68\,\mathrm{MeV}\,, \qquad M_\pi = M_{\pi^0} = 134.98\,\mathrm{MeV}\,, \\ M_{\pi^\pm} &= 139.57\,\mathrm{MeV}\,, \qquad m_e = 0.511\,\mathrm{MeV}\,, \\ F_\pi &= 92.4\,\mathrm{MeV}\,, \qquad F_K = 1.22\,F_\pi\,. \end{aligned} \tag{D.1}$$

The K_{e3} form factor is parameterized by

$$f_+(t) = f_+(0)\left[1 + \lambda_+ \frac{t}{M^2_{\pi^\pm}} + \lambda''_+ \frac{t^2}{M^4_{\pi^\pm}} + \cdots\right]\,. \tag{D.2}$$

As explained in the main text, the precise values of $f_+(0)$ and λ_+ do not matter in the present context. For numerical evaluations, we use the parameter-free one-loop result including isospin corrections [39]

$$f_+^{K^+\pi^0}(0) = 1.022 \times f_+^{K^0\pi^-}(0) = 0.998\,. \tag{D.3}$$

We stick to the low-energy constants chosen in [20],

$$L^{\mathrm{r}}_9(M_\rho) = 6.3\times10^{-3}\,, \quad L^{\mathrm{r}}_{10}(M_\rho) = -4.9\times10^{-3}\,, \tag{D.4}$$

which lead to a central value for λ_+ at one loop of

$$\lambda^{\mathrm{c}}_+ = 0.0294\,. \tag{D.5}$$

We express the low-energy constants in the following, scale independent form [18]:

$$\begin{aligned} \bar{L}_9 &= L^{\mathrm{r}}_9(\mu) - \frac{1}{512\pi^2}\log\frac{M_\pi^2 M_K^4 M_\eta^2}{\mu^8}\,, \\ \bar{L}_{10} &= L^{\mathrm{r}}_{10}(\mu) + \frac{1}{512\pi^2}\log\frac{M_\pi^2 M_K^4 M_\eta^2}{\mu^8}\,. \end{aligned} \tag{D.6}$$

References

1. F.E. Low, Phys. Rev. **110**, 974 (1958)
2. H.W. Fearing, E. Fischbach, J. Smith, Phys. Rev. Lett. **24**, 189 (1970)
3. H.W. Fearing, E. Fischbach, J. Smith, Phys. Rev. D **2**, 542 (1970)
4. M.G. Doncel, Phys. Lett. B **32**, 623 (1970)
5. V.N. Bolotov et al., Sov. J. Nucl. Phys. **44**, 68 (1986) [Yad. Fiz. **44**, 108 (1986)]
6. V.V. Barmin et al., Sov. J. Nucl. Phys. **53**, 606 (1991) [Yad. Fiz. **53**, 981 (1991)]
7. Particle Data Group, W.M. Yao et al., J. Phys. G **33**, 1 (2006)
8. V.N. Bolotov et al., arXiv:hep-ex/0510064
9. F. Romano, P. Renton, B. Aubert, A.M. Burban-Lutz, Phys. Lett. B **36**, 525 (1971)
10. D. Ljung, D. Cline, Phys. Rev. D **8**, 1307 (1973)
11. NA48/2 Collaboration, private communication
12. KEK-E470 Collaboration, S. Shimizu, private communication
13. KTeV Collaboration, A. Alavi-Harati et al., Phys. Rev. D **64**, 112 004 (2001) [arXiv:hep-ex/0106062]
14. NA48 Collaboration, A. Lai et al., Phys. Lett. B **605**, 247 (2005) [arXiv:hep-ex/0411069]
15. KTeV Collaboration, T. Alexopoulos et al., Phys. Rev. D **71**, 012 001 (2005) [arXiv:hep-ex/0410070]
16. S. Weinberg, Physica A **96**, 327 (1979)
17. J. Gasser, H. Leutwyler, Nucl. Phys. B **250**, 465 (1985)
18. J. Bijnens, G. Ecker, J. Gasser, Nucl. Phys. B **396**, 81 (1993) [arXiv:hep-ph/9209261]
19. B.R. Holstein, Phys. Rev. D **41**, 2829 (1990)
20. J. Gasser, B. Kubis, N. Paver, M. Verbeni, Eur. Phys. J. C **40**, 205 (2005) [arXiv:hep-ph/0412130]
21. V.V. Braguta, A.A. Likhoded, A.E. Chalov, Phys. Rev. D **65**, 054 038 (2002) [arXiv:hep-ph/0106147]
22. V.V. Braguta, A.A. Likhoded, A.E. Chalov, Phys. Rev. D **68**, 094 008 (2003) [arXiv:hep-ph/0305067]
23. E.H. Müller, B. Kubis, U.-G. Meißner, Eur. Phys. J. C **48**, 427 (2006) [arXiv:hep-ph/0607151]
24. A.A. Poblaguev, Phys. Atom. Nucl. **62**, 975 (1999) [Yad. Fiz. **62**, 1042 (1999)]
25. J. Wess, B. Zumino, Phys. Lett. B **37**, 95 (1971)
26. E. Witten, Nucl. Phys. B **223**, 422 (1983)
27. H.W. Fearing, S. Scherer, Phys. Rev. D **53**, 315 (1996) [arXiv:hep-ph/9408346]
28. J. Bijnens, G. Colangelo, G. Ecker, JHEP **9902**, 020 (1999) [arXiv:hep-ph/9902437]
29. O.P. Yushchenko et al., Phys. Lett. B **589**, 111 (2004) [arXiv:hep-ex/0404030]
30. KTeV Collaboration, T. Alexopoulos et al., Phys. Rev. D **70**, 092 007 (2004) [arXiv:hep-ex/0406003]

31. NA48 Collaboration, A. Lai et al., Phys. Lett. B **604**, 1 (2004) [arXiv:hep-ex/0410065]
32. KLOE Collaboration, F. Ambrosino et al., Phys. Lett. B **636**, 166 (2006) [arXiv:hep-ex/0601038]
33. W.J. Marciano, A. Sirlin, Phys. Rev. Lett. **71**, 3629 (1993)
34. V. Cirigliano, M. Knecht, H. Neufeld, H. Rupertsberger, P. Talavera, Eur. Phys. J. C **23**, 121 (2002) [arXiv:hep-ph/0110153]
35. V. Cirigliano, H. Neufeld, H. Pichl, Eur. Phys. J. C **35**, 53 (2004) [arXiv:hep-ph/0401173]
36. T. Kinoshita, J. Math. Phys. **3**, 650 (1962)
37. T.D. Lee, M. Nauenberg, Phys. Rev. **133**, B1549 (1964)
38. J. Bijnens, L. Girlanda, P. Talavera, Eur. Phys. J. C **23**, 539 (2002) [arXiv:hep-ph/0110400]
39. J. Gasser, H. Leutwyler, Nucl. Phys. B **250**, 517 (1985)